*Article*

# Simulation of Sediment Yield in a Semi-Arid River Basin under Changing Land Use: An Integrated Approach of Hydrologic Modelling and Principal Component Analysis

**Charles Gyamfi \*, Julius M. Ndambuki and Ramadhan W. Salim**

Department of Civil Engineering, Tshwane University of Technology, Private Bag X680, Pretoria 0001, South Africa; jmndambuki@yahoo.co.uk (J.M.N.); SalimRW@tut.ac.za (R.W.S.)
\* Correspondence: gyamficharles84@yahoo.com; Tel.: +27-83-433-5917

**Abstract:** Intensified human activities over the past decades have culminated in the prevalence of dire environmental consequences of sediment yield resulting mainly from land use changes. Understanding the role that land use changes play in the dynamics of sediment yield would greatly enhance decision-making processes related to land use and water resources management. In this study, we investigated the impacts of land use and cover changes on sediment yield dynamics through an integrated approach of hydrologic modelling and principal component analysis (PCA). A three-phase land use scenario (2000, 2007 and 2013) employing the "fix-changing" method was used to simulate the sediment yield of the Olifants Basin. Contributions in the changes in individual land uses to sediment yield were assessed using the component and pattern matrixes of PCA. Our results indicate that sediment yield dynamics in the study area is significantly attributed to the changes in agriculture, urban and forested lands. Changes in agriculture and urban lands were directly proportional to sediment yield dynamics of the Olifants Basin. On the contrary, forested areas had a negative relationship with sediment yield indicating less sediment yield from these areas. The output of this research work provides a simplistic approach of evaluating the impacts of land use changes on sediment yield. The tools and methods used are relevant for policy directions on land and water resources planning and management.

**Keywords:** land use-land cover change (LULCC); Olifants Basin; principal component analysis; sediment yield; SWAT

## 1. Introduction

Sedimentation is one of the key environmental problems arising from soil erosion and is widely acknowledged throughout the world owing to its ramifications on water resources quality, reservoir capacity reduction and low agricultural productivity due to the removal of top rich nutrient soils [1–10]. The multiplicative effect of sediment loads causes a huge burden on water infrastructures through the upsurge of recurring costs, especially in the case of raw water abstraction and treatment for community water supply. The interplay between geology, soil texture, topography, land use and climate change are noted as stimuli to the quantity of sediment loads generated within and transported out of watersheds [3,11]. Current studies indicate that sediment production and transport in watersheds are intrinsically linked to the synergic forces of climate and land use [12–14]. With the advent of climate change some proponents are of the view that increases in temperature and alterations in precipitation will affect the extent, frequency and magnitude of sediment fluxes [14–16]. Others also are of the view that land use change and soil management practices wield a greater influence on sediment

fluxes compared to climate variability [17–21]. Nonetheless, the degree to which the frequency and magnitude of sediment fluxes are impacted upon by climate change and land use still remains a subject of debate.

In recent times, the impacts of land use/cover change (LULCC) on hydrology have gained tremendous concern on the part of researchers [22–25], with little consideration accorded sediment fluxes [5,10]. This in part is explained by the extreme difficulties in measuring sediment fluxes and hence the unavailability of required sediment data for further studies [26,27]. The spatial extent of soil erosion causing sediment fluxes presents many difficulties for its continuous monitoring amidst scarce human resources, site remoteness and logistical constraints [28]. In the event of these happenings, the use of hydrologic and sediment yield models in predicting sediment yields is fast gaining recognition among researchers [5,27,29,30]. These scientific tools are built on robust mathematical modelling techniques with capabilities to demonstrate the spatial and temporal dynamics of sediment fluxes [31,32]. Although sediment data remains a hindrance, efforts both in the past and present have proven satisfactory in the use of limited sediment data through the application of distributed hydrologic models.

Oeurng et al. [29] investigated sediment yields in the Save catchment of Coteaux Gascogne, France using a limited set of suspended sediment concentration data for the period $2007-2009$. In their work, they used the SWAT hydrologic model. Despite the short span of observed suspended sediment data, the model performance in simulating the sediment yield of the basin was within acceptable limits. Equally, in the Maybar gauged watershed of Ethiopia, Yesuf et al. [33] simulated sediment yield with 14 years of historical sediment data using SWAT and concluded with a satisfactory model application. Similarly, Setegn et al. [34] also applied the SWAT model in the assessment of sediment yield of the Anjeni gauged watershed in Ethiopia. In their study, historical records of sediment for ten years were used. Findings from their study indicate the capabilities of the SWAT model in simulating sediments with acceptable model performance statistics. In China, a series of work on sediment yield have been carried out using the SWAT hydrologic model with relatively limited data [6,35]. The foregone discussions demonstrate the capabilities of the SWAT model in simulating sediment yield within basins with a limited set of observed data and in different geographic jurisdictions.

In South Africa, sediment studies have in the past been done through reservoir sediment surveys and empirical approaches [11,36]. However, these methods of sediment studies are capital intensive and human resource demanding. More so in most parts of Africa, the requisite sophistication for the execution of accurate reservoir sediment surveys are lacking. Against the backdrop of these challenges and with the advent of more sophisticated physically based models, the approach to watershed studies, especially sediment yield modelling, needs to evolve to provide real-time information relevant to remediation and conservation strategies. Thus, the objective of the present study was to apply the SWAT hydrologic model to a large semi-arid basin in Southern Africa with limited data in order to (a) assess the impacts of LULCCs on sediment yield; (b) quantify the annual sediment yield of the study basin over a period of time; and (c) identify sediment-prone areas within the basin. The approaches espoused in this study overcome the limitations of the conventional methods of reservoir sediment surveys which are inept in determining the spatio-temporal dynamics of sediment yield at the basin scale to warrant the implementation of conservation measures.

## 2. Materials and Methods

### 2.1. Description of the Study Location

The Olifants River originates from Trichardt town to the east of Johannesburg in the province of Gauteng and then flows in northeasterly direction through the provinces of Mpumalanga and Limpopo with a total length of about 770 km. It finally flows through the Kruger National Park (KNP) and empties into the Massingir dam in Mozambique. The basin drains an area of approximately $73.7 \times 10^3$ km$^2$. However, this study limits its investigations to the area extending from the upper

Olifants to gauge station B7H015 (Figure 1) which drains an area of $50.02 \times 10^3$ km$^2$. Major tributaries of the Olifants River are Wilge, Moses, Elands, Ga-Selati, Letaba on the left bank and Klein Olifant, Steelpoort and Blyde on the right bank [37]. Geographically, the basin spans between 22.6° S–26.5° S latitudes and 28.3° E–31.9° E longitudes. The climate of the basin is characterized by the inter tropical convergence zone (ITCZ) with seasonal rainfall occurring during the months of October to April. The mean annual rainfall is 630 mm with peaks in January [38]. Rainfall in the basin varies both in space and time with a coefficient of variation of 24% [39]. Temperatures range from 18 °C–34 °C in summer and 5 °C–26 °C in winter. Geology of the basin is mainly characterized by igneous and metamorphic rocks whose formations are associated with African and Post-African planation surfaces which were formed through uplift. The basin is underlain by five major soil types, namely: cambic arenosols, chromic luvisols, chromic vertisols, orthic acrisols and rhodic ferralsols [40]. Land uses include mining, agriculture, forestry, animal husbandry and residential purposes. Agricultural activity is dominant providing employment to a majority of the rural inhabitants. Agriculture, together with other economic activities in the basin, contributes 5% to the total GDP of South Africa [41]. Soil erosion and sedimentation resulting from anthropogenic activities mainly in land use practices and management is reported as a major environmental concern within the basin [42]. However, no major strategies are in place to monitor and check sediment yields in the basin. This in part is attributed to scarce human resources, site remoteness and logistical constraints which delimit the availability of sediment data from which scientific knowledge could be gained to inform policy actions.
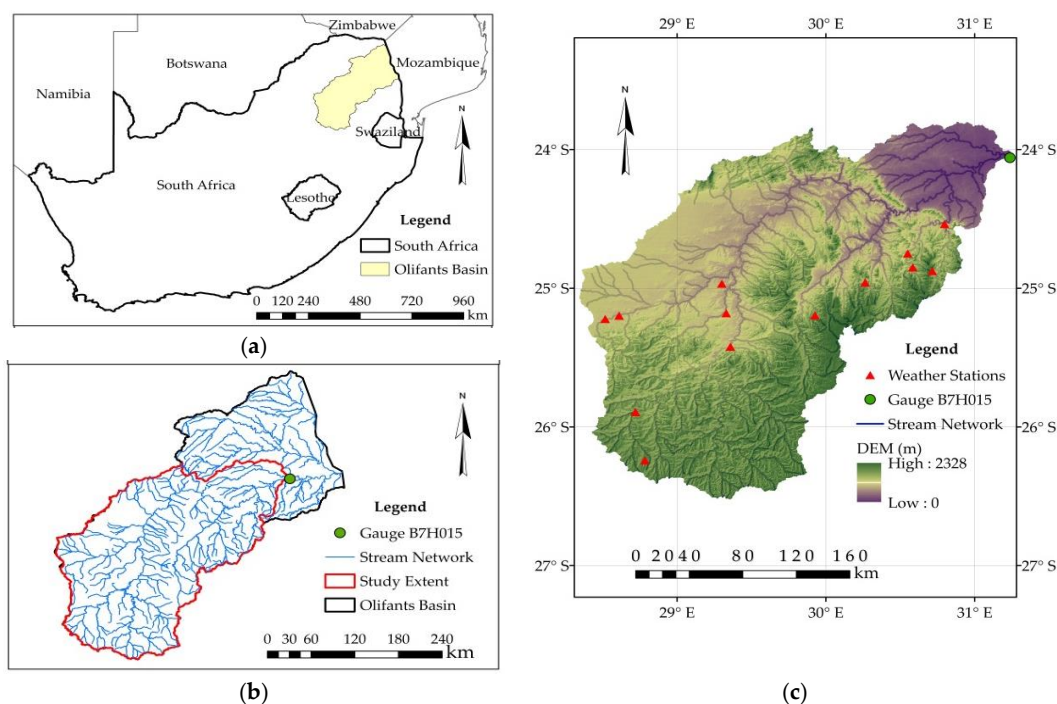


**Figure 1.** Study location within the context of South Africa (**a**), study extent (**b**) and weather stations (**c**).

*2.2. Model Selection and Description*

The Soil and Water Assessment Tool (SWAT) [3,5,10,22–25,29,33,43] was selected to model the sediment yield of the Olifants Basin owing to its acknowledged capabilities in modelling watershed hydrology and sediment yield coupled with its application in different geographic jurisdictions. The SWAT model is a continuous, long-term, physically based distributed model developed to predict the impact of management practices on water, chemical yields and sediments in large complex watersheds [44,45]. The basic operational unit of the model is the hydrologic response unit (HRUs) which consists of an area of homogeneous land use, management and soil characteristics. The HRUs

are nested within sub-basins and hence simulations are aggregated at the HRUs and then unto the sub-basins. SWAT is capable of integrating different spatial data, thus making it versatile in its application.

Sediment fluxes in SWAT are modelled using Equation (1), the Modified Universal Soil Loss Equation (MUSLE) following the mathematical formulation of Williams [46];

$$\text{Sed} = 11.8 \left(Q_{surf} \cdot q_{peak} \cdot area_{hru}\right)^{0.56} \cdot K_{USLE} \cdot C_{USLE} \cdot P_{USLE} \cdot LS_{USLE} \cdot CFRG \tag{1}$$

where, Sed is the sediment yield on a given day (metric tons), $Q_{surf}$ is the surface runoff volume (mm/ha), $q_{peak}$ is the peak runoff rate (m$^3$/s), $area_{hru}$ is the area of the HRU (ha), $K_{USLE}$ is USLE soil erodibility factor (0.013 metric ton m$^2$ h/(m$^3$-metric ton cm)), $C_{USLE}$ is the USLE cover and management factor, $P_{USLE}$ is the USLE support practice factor, $LS_{USLE}$ is the USLE topographic factor and CFRG is the coarse fragment factor.

The peak runoff rate $\left(q_{peak}\right)$ is estimated using the modified rational method. An underlying assumption of the modified rational method states that for a given rainfall of intensity i beginning at time t = 0 and continuing indefinitely, the rate of runoff thus increases till the time of concentration ($t_{conc.}$) when the entire subbasin area contributes flow to the basin outlet. The rational formula for $q_{peak}$ is estimated using Equation (2) [47]:

$$q_{peak} = \frac{\alpha_{tc} \cdot Q_{surf} \cdot \text{Area}}{3.6 t_{conc.}} \tag{2}$$

where $q_{peak}$ is the peak runoff rate (m$^3$/s), $\alpha_{tc}$ is the fraction of daily rainfall that occurs during the time of concentration, $Q_{surf}$ is the surface runoff (mm), Area is the subbasin area (km$^2$), $t_{conc.}$ is the time of concentration for the subbasin (h) and 3.6 is a unit conversion factor.

After generation of peak runoff, sediment fluxes are simulated as a function of two principal processes: degradation and deposition. These processes dictate the amount of sediments entrained or transported out of the watershed. Sediment deposited is estimated using the stream power theorem of Bagnold [48] as used by Williams [49] and given in Equation (3):

$$\text{Sed}_\Phi = \left(conc_{sed,ch,i} - conc_{sed,ch,mx}\right) \cdot V_{ch} \tag{3}$$

where $\text{Sed}_\Phi$ is the amount of sediment deposited (metric tons), $conc_{sed,ch,i}$ is the initial sediment concentration in the reach (ton/m$^3$ or kg/L), $conc_{sed,ch,mx}$ is the maximum concentration of the sediment that can be transported by the water (ton/m$^3$ or kg/L) and $V_{ch}$ is the volume of water in the reach segment (m$^3$).

The amount of sediment entrained is subsequently estimated using Equation (4):

$$\text{Sed}_\tau = \left(conc_{sed,ch,mx} - conc_{sed,ch,i}\right) \cdot V_{ch} \cdot K_{CH} \cdot C_{CH} \tag{4}$$

where $\text{Sed}_\tau$ is the amount of sediment re-entrained (metric tons), $conc_{sed,ch,i}$ is the initial sediment concentration in the reach (ton/m$^3$ or kg/L), $conc_{sed,ch,mx}$ is the maximum concentration of the sediment that can be transported by the water (ton/m$^3$ or kg/L) and $V_{ch}$ is the volume of water in the reach segment (m$^3$), $K_{CH}$ is the channel erodibility factor and $C_{CH}$ is the channel cover factor.

For further reading on the SWAT model, one is referred to Neistch et al. [47] and online resources at http://swat-model.tamu.edu/.

## 2.3. Data Requirement and Sources

### 2.3.1. Hydro-Meteorological and Sediment Data

Climatic data required to set up the SWAT model are daily rainfall, maximum and minimum temperatures, solar radiation, wind speed and humidity. These datasets were obtained from thirteen weather stations (Figure 1c) maintained by the South African Weather Service (SAWS) for the period 1980−2013. The climatic data were augmented with information from the weather stations maintained by the Department of Water and Sanitation (DWS) and Climate Forecast System Reanalysis (CFSR) database. Stream discharges (1980−2013) and sediment data (1993−1999) for gauge station B7H015 were respectively obtained from the Hydrological Department and the Institute of Water Quality Studies (IWQS), all under DWS for calibration and validation of the SWAT setup model.

### 2.3.2. Soil Data

Soil physico-chemical and hydrological properties were obtained from various FAO-UNESCO soil databases [40,50] and the land type survey staff [51]. From the FAO soil database, attributes for each soil polygon, namely, soil texture, Hydrological Soil Group (HSG), soil depth, rock fragments and organic carbon content, were obtained. The databases are considered the single most comprehensive available resource with vast database on soil attributes for Africa and the world [52]. Field soil samples were also analyzed for particle size and organic carbon content to supplement secondary data sources. A subset of the soil of the Olifants Basin (Figure 2) indicates five major soil types: cambic arenosols, chromic luvisols, chromic vertisols, orthic acrisols and rhodic ferralsols [40]. The distribution of the soil types indicates chromic luvisols as the dominant soil covering 38.81% of the watershed. It is followed by cambic arenosols (33.03%) and chromic vertisols (21.21%). Orthic acrisols and rhodic ferralsols constitute a marginal proportion of 5.77% and 1.18%, respectively. Shown in Table 1 are some selected physical and hydrological properties for the major soil groups found in the Olifants Basin. All the attributes of the soils (soil texture, Hydrological Soil Group (HSG), soil depth, rock fragments and organic carbon content) were captured in a database using GIS which provided a link for usage in SWAT. The value fields that ensured the proper recall of gridded soil information were the serial number (SNUM) and the FAO soil code.
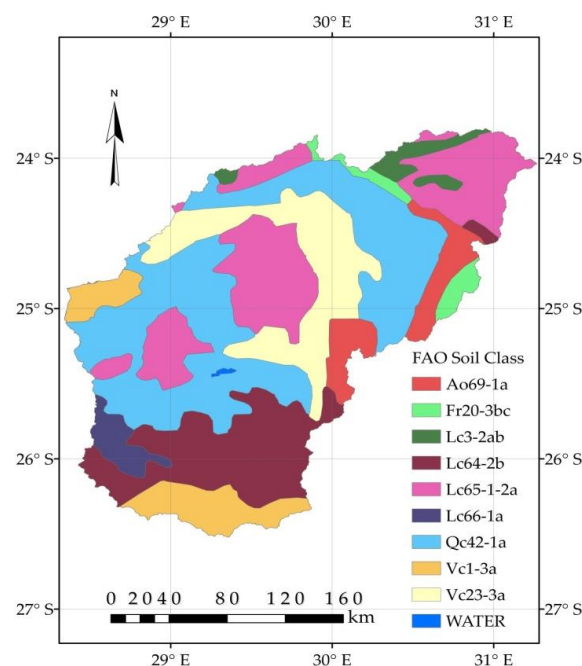


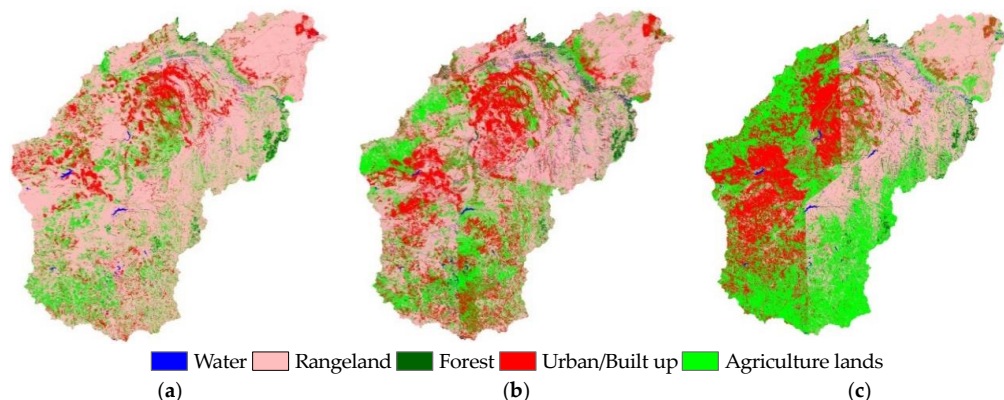**Figure 2.** Major soil types of the Olifants Basin.

**Table 1.** Some physical and hydrological properties of major soils in the Olifants Basin.

| Soil Type | FAO Code | Hydrologic Group | Texture | BD (g/cm$^3$) * | AWC (mm/mm) * |
|---|---|---|---|---|---|
| Cambic Arenosols | Qc42-1a | C | Sandy loam | 1.45 | 0.08 |
| Chromic Luvisols | Lc65-1-2a | C | Sandy loam | 1.45 | 0.14 |
| | Lc3-2ab | C | Sandy Clay Loam | 1.50 | 0.18 |
| | Lc66-1a | C | Sandy Loam | 1.45 | 0.14 |
| | Lc64-2b | C | Sandy Clay Loam | 1.50 | 0.16 |
| Chromic Vertisols | Vc23-3a | D | Clay | 1.60 | 0.14 |
| | Vc1-3a | D | Clay | 1.65 | 0.13 |
| Orthic Acrisols | Ao69-1a | C | Sandy Loam | 1.50 | 0.01 |
| Rhodic Ferralsols | Fr20-3bc | C | Clay | 1.20 | 0.16 |

Note: BD, Bulk density; AWC, Available Water Content; * Average for layers 1 and 2 of soil profile.

### 2.3.3. Land Use/Cover Dataset

The spatial land use/cover dataset (Figure 3) used was obtained through a supervised classification of Landsat 7 ETM/ETM+ level 1 terrain-corrected satellite images. The images of spatial resolution 30 m were obtained from the Global Visualization Viewer (GLOVIS) for Path/Row; 168/077, 169/077, 169/078, 170/077 and 170/078 for three epochs of 2000, 2007 and 2013. The images were classified into five-level 1 classes (Table 2) based on the land cover and land use classification system developed by Anderson et al. [53] for the interpretation of remote sensor data at various scales and resolutions.



Water　Rangeland　Forest　Urban/Built up　Agriculture lands
(**a**)　　　　　　　　　　　　(**b**)　　　　　　　　　　　　(**c**)

**Figure 3.** Classified land use maps for (**a**) 2000; (**b**) 2007; and (**c**) 2013 in the Olifants Basin.

**Table 2.** Land cover classification scheme.

| Land Cover Class | Description |
|---|---|
| Urban/Built up | Residential, commercial services, industrial, transportation, communications, mixed urban or built up lands |
| Agricultural lands | Crop fields and pastures |
| Forest | Deciduous, evergreen and mixed forest |
| Water | Lakes, reservoirs, stream |
| Rangeland | Herbaceous, shrub and brush and mixed rangeland |

### 2.3.4. Digital Elevation Model (DEM) and Basin Discretization

A three-arc second (90 m × 90 m) pixel resolution SRTM DEM (Figure 1c) obtained from the Consortium for Spatial Information of the Consultative Group of International Agricultural Research (CGIAR-CSI) formed the basis for the watershed delineation of the study area and further estimation

of geomorphologic characteristics. Three slope classes (Figure 4a)—level to gently undulating (<8%), rolling to hilly (8%−30%) and steeply dissected to mountainous (>30%)—were extracted based on FAO classification [54]. The multiple slope classes approach catered to the different slopes that exist within the area unlike using a single slope approach. The area proportion in terms of the classified slopes were 76.57% for level to gently undulating terrain (<8%); 18.26% for rolling to hilly terrain (slope class 8%−30%) and 5.17% being steeply dissected to mountainous (slope class > 30%). Inference from the classified slopes generally portrays that the Olifants watershed has varying terrain with approximately 24% of the area having slopes greater than 8%. The steep slopes (>30%) were mainly located in the region of the escarpment. Subsequently, the basin was discretized into 23 sub-basins (Figure 4b) with hydrologic response thresholds (HRTs) of 10%, 10% and 10% for land use, soils and slopes, respectively. The defined thresholds ensure a unique combination of land use, soils and slopes in the eventual determination of hydrologic response units (HRUs) by simplifying catchment processes.
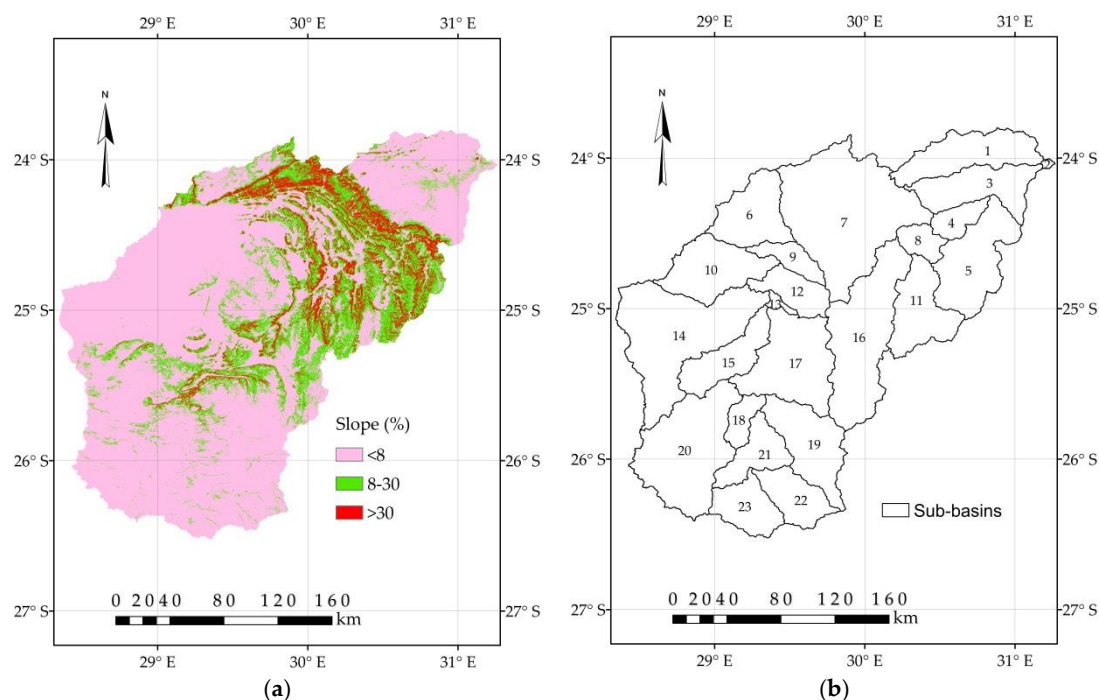


**Figure 4.** Discretized (**a**) slope classes and (**b**) sub-basins of the Olifants Basin.

*2.4. Parameter Sensitivity Analysis, Calibration and Validation*

Sediment fluxes are influenced by a large number of parameters; hence, sensitivity analysis to identify the most crucial parameters became essential. The global sensitivity analysis employing SUFI-2 algorithm in SWAT-CUP 2012 version 5.1.6 (Eawag: Swiss Federal Institute of Aquatic Science and Technology, Dübendorf, Switzerland) environment was used [55] in selecting the most sensitive parameters to sediment fluxes. The global sensitivity analysis considers the sensitivity of one parameter in relation to other parameters subjected to the sensitivity analysis. A total of fourteen parameters gathered from the literature to influence sediment fluxes were subjected to the sensitivity analysis. The sensitivity of a parameter was measured by *t*-stat and its significance by the *p*-value. The higher the absolute value of *t*-stat for a parameter, the more significant that parameter in the sediment generation and transport process. Following sensitivity analysis, the model was initially calibrated (1988–2001) and validated (2002–2013) for streamflow [5,56]. After a successful calibration of streamflow, the model was subsequently calibrated (1994−1995) and validated (1996–1997) for sediment. Calibration and validation of streamflow and sediment were done through an auto-calibration process in SWAT-CUP 2012.

## 2.5. Model Performance Statistics

The performance of the model in simulating sediment yield was evaluated using both statistical and graphical means. The model was evaluated against four objective functions commonly used in the assessment of model performance [29,56,57].

(a) Nash-Sutcliffe (NSE): This statistics determines the relative magnitude of the residual variance compared to the observed data variance [58]. NSE ranges from $-\infty$ to 1, where 1 denotes perfect agreement between simulated and observed variables. NSE is formulated in Equation (5) as:

$$\text{NSE} \ = \ 1 - \frac{\sum_{i=1}^{n} \left(O_i - S_i\right)^2}{\sum_{i=1}^{n} \left(O_i - \overline{O}\right)^2} \tag{5}$$

(b) Coefficient of determination ($R^2$): It measures the proportional variation in the simulated variable explainable by the observed variable and gives an indication of the linear relationship between the simulated and observed variables. $R^2$ is estimated using Equation (6):

$$R^2 \ = \ \left[ \frac{\sum_{i=1}^{n} \left(O_i - S_i\right)\left(S_i - \overline{S}\right)}{\left(\sum_{i=1}^{n} \left(O_i - \overline{O}\right)^2\right)^{0.5} \left(\sum_{i=1}^{n} \left(S_i - \overline{S}\right)^2\right)^{0.5}} \right]^2 \tag{6}$$

(c) Percent Bias (PBIAS): PBIAS is a measure of how much (in percentage) the observed variable is either underestimated or overestimated [59]. It is calculated using Equation (7):

$$\text{PBIAS} \ = \ \frac{\sum_{i=1}^{n} \left(O_i - S_i\right)}{\sum_{i=1}^{n} O_i} \ \times \ 100 \tag{7}$$

(d) RMSE observations standard deviation ratio (RSR): RSR standardizes the root mean square error (RMSE) using the observation standard deviations. RSR is expressed in Equation (8) as:

$$\text{RSR} \ = \ \frac{\text{RMSE}}{\text{STD}_{\text{obs}}} \ = \ \frac{\sqrt{\sum_{i=1}^{n} \left(O_i - S_i\right)^2}}{\sqrt{\sum_{i=1}^{n} \left(O_i - \overline{O}\right)^2}} \tag{8}$$

where $O_i$ is observed variable, $S_i$ is simulated variable, $\overline{O}$ is mean of observed variable, $\overline{S}$ is mean of simulated variable, n is number of observations under consideration, RMSE is root mean square error, $\text{STD}_{\text{obs}}$ is standard deviation of observed variable.

## 2.6. Model Application and Statistical Analysis

To assess the impacts of LULCCs on sediment yield of the Olifants Basin, the "fix-changing" method was used [10,43,60–62]. The "fix-changing" method employs variation in land use data while keeping constant other spatial variables for the different epochs under consideration. In this regard, the calibrated model was run for each of the land use maps (2000, 2007 and 2013) from January 1985 to December 2013 while keeping constant the DEM, climatological parameters and soil data. Simulated results were further used to evaluate the impact of LULCCs on sediment yield components at the basinal and sub-basinal scales. The changes observed in the sediment yield components were mapped out at the sub-basinal scale using ArcGIS 10.2 to aid in the decision-making process. Simple statistics of minimum, maximum, mean and standard deviation were used to indicate sediment dynamics at the sub-basinal scale. Further analyses employing principal component analysis (PCA) were used to examine the contributions in the changes of individual land uses on sediment yield. This was achieved by analyzing the component and pattern matrixes of the PCA. Changes in agriculture, rangeland, urban and forest constituted the predictor variables for the PCA analysis with response variable being sediment yield. All statistical analyses were carried out at a significance level of 0.05. SPSS 16.0

(IBM SPSS, Chicago, MI, USA) was used for the statistical analysis and graphical presentations done with MS excel 2010.

## 3. Results and Discussion

### 3.1. Sensitivity Analysis

Summarized in Table 3 are the identified influential parameters to streamflow and sediment yield with their range and fitted values. Streamflow was highly sensitivity to runoff curve number (CN2) with a *t*-stat of |37.72| and significant value at $p < 0.05$. As CN2 is a function of land use/cover (LULC) influencing other parameters such as antecedent moisture content, it could be inferred that changes in LULC will have a greater implication on surface runoff and sediment yield. Equally identified sensitive parameters to streamflow were the base flow alpha factor for bank storage (ALPHA_BNK, *t*-stat = |6.97|, $p < 0.05$), soil evaporation compensation factor (ESCO, *t*-stat = |5.57|, $p < 0.05$), soil available water capacity (SOIL_AWC, *t*-stat = |4.13|, $p < 0.05$), groundwater delay (GW_DELAY, *t*-stat = |3.02|, $p < 0.05$) and groundwater "revap" coefficient (GW_REVAP, *t*-stat = |2.34|, $p < 0.05$). Sediment generation in the basin is influenced by both channel and landscape parameters. The most sensitive channel parameters to sediment yield were the linear parameter for sediment routing (SPCON, *t*-stat = |9.95|, $p < 0.05$), exponent parameter for sediment routing (SPEXP, *t*-stat = |7.46|, $p < 0.05$) and the channel cover factor (CH_COV, *t*-stat = |3.92|, $p < 0.05$). Landscape influential parameters were support practice (USLE_P, *t*-stat = |2.92|, $p < 0.05$) and land cover (USLE_C, *t*-stat = |2.38|, $p < 0.05$) factors.

**Table 3.** Calibrated sensitive parameters to streamflow and sediment.

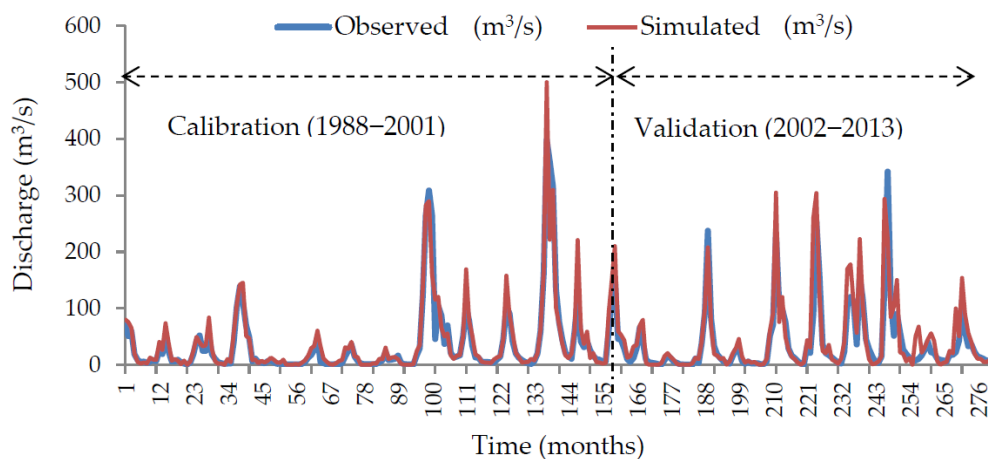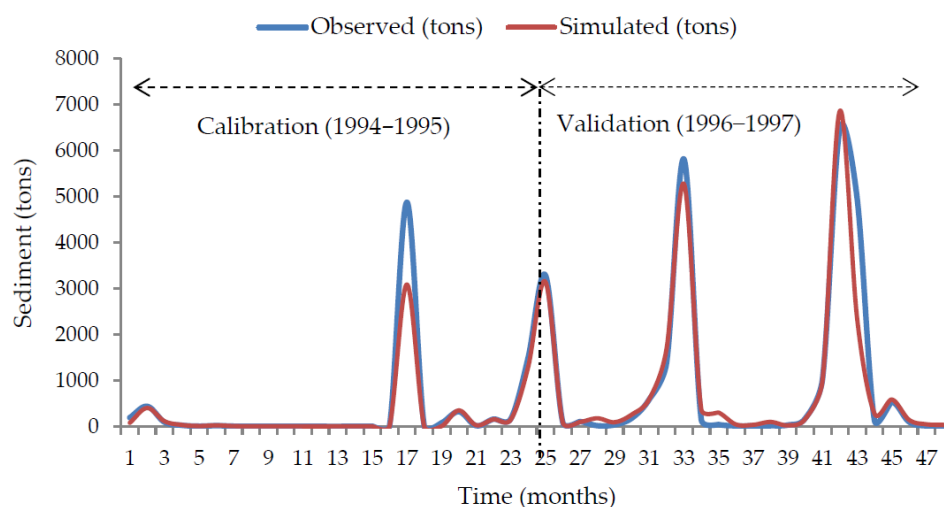| Process | Parameter [a] | Global Sensitivity | | | Range | Fitted Values |
|---|---|---|---|---|---|---|
| | Code | *t*-stat [b] | *p*-Value | Rank | | |
| Streamflow | CN2 | 37.72 | 0.00 | 1 | 35−98 | 65 |
| | ALPHA_BNK | 6.97 | 0.00 | 2 | 0−1 | 0.39 |
| | ESCO | 5.57 | 0.00 | 3 | 0−1 | 0.67 |
| | SOIL_AWC | 4.13 | 0.00 | 4 | 0−1 | 0.20 |
| | GW_DELAY | 3.02 | 0.00 | 5 | 0−500 | 345 |
| | GW_REVAP | 2.34 | 0.02 | 6 | 0.02−0.2 | 0.15 |
| Sediment | SPCON | 9.95 | 0.00 | 1 | 0−0.01 | 0.0001 |
| | SPEXP | 7.46 | 0.00 | 2 | 1−1.5 | 1 |
| | CH_COV | 3.92 | 0.00 | 3 | −0.001−1 | 0.45 |
| | USLE_P | 2.92 | 0.00 | 4 | 0−1 | 0.53 |
| | USLE_C | 2.38 | 0.02 | 5 | 0.001−0.5 | 0.20 |
| | CH_EROD | 2.09 | 0.04 | 6 | −0.05−0.6 | 0.37 |

[a] CN2, surface runoff number; ALPHA_BNK, base flow alpha factor for bank storage; ESCO, soil evaporation compensation factor; SOIL_AWC, soil available water capacity; GW_DELAY, groundwater delay; GW_REVAP, groundwater "revap" coefficient; SPCON, linear parameter for sediment routing; SPEXP, exponent parameter for sediment routing; CH_COV, channel cover factor; USLE_P, USLE support practice factor; USLE_C, Min. value of USLE factor applicable to land cover/plant; CH_EROD, channel erodibility factor; [b] Values represent absolute numbers.

### 3.2. Calibration and Validation

The model performance statistics for streamflow and sediment are shown in Table 4. Figure 5 shows simulated and observed streamflow for both calibration and validation periods. It is evident from Table 4 and Figure 5 that the model simulated well the observed discharge during both calibration and validation periods. The NSE values during both calibration and validation were over 0.65 and $R^2$ over 0.75. Although the model performance was good, streamflow was overestimated during both calibration and validation stage with PBIAS of −11.49% and −20.69% respectively. RSR value for calibration was 0.34 and 0.57 for validation. Sediment was also satisfactorily modelled with simulated sediment matching fairly with the observed (Figure 6).

**Table 4.** Performance statistics of calibrated and validated model.

| Objective Function | Streamflow | | Sediment | |
|---|---|---|---|---|
| | Calibration | Validation | Calibration | Validation |
| NSE | 0.88 | 0.67 | 0.66 | 0.64 |
| $R^2$ | 0.89 | 0.78 | 0.68 | 0.60 |
| PBIAS (%) | −11.49 | −20.69 | 27.36 | 39.73 |
| RSR | 0.34 | 0.57 | 0.57 | 0.59 |



**Figure 5.** Calibration and validation of streamflow.



**Figure 6.** Calibration and validation of sediment yield.

### 3.3. Land Use/Land Cover Changes (LULCC) Impacts on Sediment Yield

Table 5 summarizes changes in LULC and maximum annual sediment yield of the Olifants basin for the period 2000 to 2013. It is evident that changes occurred in all land use classes. However, urban, agricultural and range lands underwent the most significant changes. Urban and agricultural areas continually increased for all the years under review. Urban area extent of 13.2% in 2000 increased to 22.4% in 2007. Urban areas gradually increased again from 22.4% in 2007 to 23.7% in 2013. Similarly, from 2000 to 2007, agricultural areas increased from 15.2% to 21.3%. Further expansion in agriculture lands were observed, increasing from 21.3% in 2007 to 35.3% in 2013. Unlike agriculture and urban areas, rangeland continually decreased from 69.2% to 52.4% between 2000 and 2007. By the end of 2013, rangeland had decreased from 52.4% in 2007 to 37.6%, making it the land use type to have undergone

the most significant reduction for the period under study. The reduction in rangelands was the result of their conversion to agriculture and urban land uses.

**Table 5.** Proportion of land use, maximum annual sediment yield and changes in these values for the Olifants Basin ($-/+$ respectively indicates reduction and increase in land use type/sediment yield).

| Time Period | LULC Change (%) * | | | | Sediment Yield (t/km$^2$.a) |
|---|---|---|---|---|---|
| | **FRST** | **URHD** | **AGRL** | **RNGB** | |
| 2000 | 1.6 | 13.2 | 15.2 | 69.2 | 946.76 |
| 2007 | 2.8 | 22.4 | 21.3 | 52.4 | 1110.02 |
| 2013 | 2.3 | 23.7 | 35.3 | 37.6 | 1408.27 |
| 2000−2007 | +1.1 | +9.2 | +6.1 | −16.8 | +163.27 |
| 2007−2013 | −0.5 | +1.3 | +14.0 | −14.8 | +298.25 |
| 2000−2013 | +0.7 | +10.5 | +20.2 | −31.6 | +461.52 |

\* FRST, Forest; URHD, Urban lands; AGRL, Agriculture; RNGB, Rangelands.

The highest sediment yield for the years 2000, 2007 and 2013 were simulated with the SWAT model (Table 5) and the sediment yield in all 23 sub-basins analyzed statistically; the results are summarized in Table 6. Considerations of the 23 sub-basins under the same climatic conditions but with different land use scenarios resulted in noticeable changes in the spatial distribution of sediment yield (Figure 7). It is evident that sediment yield varied significantly across sub-basins. Generally, sediment yields were higher in the southern areas than in the northern areas. This is mainly due to the changes in dominant land uses (i.e., rangeland, agriculture and urban) which are fairly predominant in the south. For example, the conversions of rangeland to agriculture were pronounced in the south than in the north. The changes in land uses are reflected in surface runoff responses due to the changes that are observed in canopy structure, surface runoff curve number and surface roughness whose eventual repercussion is on sediment yield [43,63,64].

**Table 6.** Summary statistics of sediment yield for the 23 discretized sub-basins of the Olifants.

| Statistics | Sediment Yield (t/km$^2$.a) | | |
|---|---|---|---|
| | **2000** | **2007** | **2013** |
| Mean | 136.90 | 173.77 | 446.49 |
| Standard Deviation | 187.16 | 226.82 | 335.75 |
| Minimum | 5.88 | 14.92 | 105.35 |
| Maximum | 946.76 | 1110.02 | 1408.27 |

The maximum sediment yield at the sub-basinal scale occurred in sub-basin 2 for all the years under review (i.e., 2000, 2007and 2013). This is possibly due to the downstream nature of the sub-basin thus causing it to receive most of the sediment generated upstream. Similarly, higher sediment yields in 2000, 2007 and 2013 are located in sub-basins 5, 15, 16; 5, 15, 23; 5, 7 and 20, respectively. The majority of these sub-basins are located in areas with rolling to hilly slopes (8%–30%) or steeply dissected slopes (>30%). This suggests that sediment yield is also influenced by the terrain of the basin. Compared with 2000 and 2007, the 2013 land use pattern had the utmost impact on the potential risk of sediment yield. The highest sediment yield for the years 2000, 2007 and 2013 were 946.76 t/km$^2$.a, 1110.02 t/km$^2$.a and 1408.27 t/km$^2$.a, respectively. Compared to the baseline in 2000, sediment yield of the basin was 163.27 t/km$^2$.a higher in 2007 and 461.52 t/km$^2$.a higher in 2013 (increases of 17.2% and 48.7%).
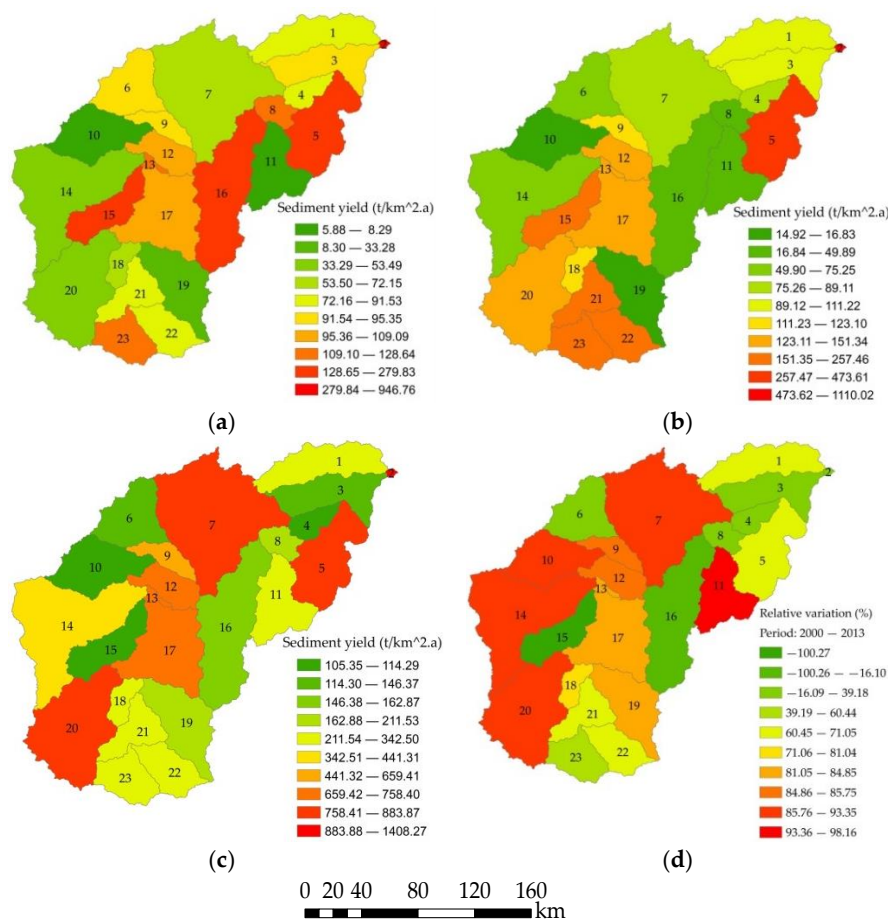
**Figure 7.** Spatial distribution of sediment yield for 2000 (**a**); 2007(**b**); 2013 (**c**); and sediment deviations for 2000−2013 (**d**).

A comparative analysis of sediment yield of the Olifants Basin with other studies in similar semi-arid large basins in Africa is presented in Table 7. Evidently, the SWAT-distributed hydrologic model gave comparable estimates of sediment fluxes. In particular, the mean sediment yield obtained in this study is in close agreement with that estimated for Vaal (125 t/km$^2$.a) and Orange (352 t/km$^2$.a) Basins in South Africa which were based on reservoir sediment surveys [65,66]. These comparisons also validate the SWAT model as a reliable tool in estimating the sediment dynamics of the Olifants Basin under contraint data conditions.

**Table 7.** Comparative analysis of sediment yield in some selected large basins in Africa.

| Country | Catchment | Area $\times 10^4$ (km$^2$) | Sediment Yield (t/km$^2$.a) | Reference |
|---|---|---|---|---|
| Kenya | Tana | 4.2 | 761.9 | Milliman and Farnsworth [67] |
| Mozambique | Kabora Bassa | 100.0 | 134.5 | Bolton [68] |
| Madagascar | Mangoky | 5.9 | 169.5 | Milliman and Farnsworth [67] |
| Madagascar | Tsiribihina | 4.5 | 266.7 | Milliman and Farnsworth [67] |
| Tanzania | Rufiji | 15.6 | 106.0 | FAO [69] |
| South Africa | Orange | 6.8 | 352.0 | Rooseboom et al. [66] |
| South Africa | Vaal | 3.7 | 125.0 | Rooseboom [65] |
| South Africa | Olifants | 5.0 | 136.9−446.5 * | This study |

* Represents range of mean sediment yield for the epochs considered in this study.

*3.4. Contributions of Individual Land Use Changes on Sediment Yield*

Figure 8 shows the PCA model constructs for sediment yield. The sediment yield model extracts two PCA components with eigenvalues ≥1 (Figure 8) based on four predictor variables (i.e., forest, urban, rangeland and agriculture). The models were constructed satisfying the requirements of Bartlett's test of sphericity (df = 6; $p < 0.05$), Kaiser-Meyer-Olkin (KMO) measure of sampling adequacy (KMO = 0.60) and determinant of 0.21. The first component explained 54.6% of the variability observed in the sediment yield (Figure 8). The addition of the second component cumulatively explained 84.7% of the variation in sediment yield resulting from individual LULC changes. The second component therefore explained 30.1% of the total variance in sediment yield. The inclusion of more models resulted in no significant improvement of the percentage variance explained (Figure 8). This implies that variation in sediment yield is influenced by two loading components. The first component of the sediment yield model (Table 8) was dominated by agriculture and urban on the positive side and forest on the negative side. In consideration of the second component, agriculture and urban land uses were dominant with both on the positive side.
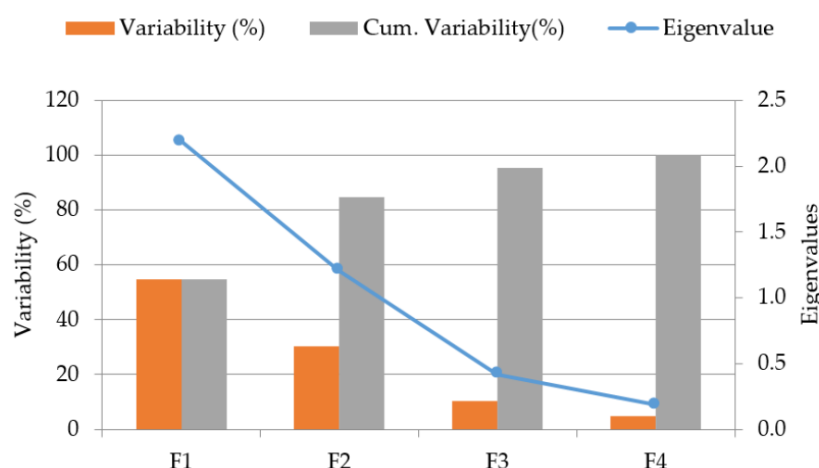


**Figure 8.** Extracted factors of the principal component analysis with scree plot.

**Table 8.** Factor loadings and pattern matrix [a].

| Predictors | Component Matrix [b] | | Pattern Matrix [c] | |
|---|---|---|---|---|
| | F(1) | F(2) | P(1) | P(2) |
| Forest | **−0.862** | −0.132 | −0.868 | −0.085 |
| Urban | **0.659** | **0.402** | 0.832 | 0.448 |
| Rangeland | −0.014 | −0.259 | −0.075 | −0.213 |
| Agriculture | **0.839** | **0.980** | 0.854 | 0.978 |

[a] The bold numerical values indicate that the PCA components are mainly loaded on the corresponding variable;
[b] F(1) and F(2) are component matrixes for components 1 and 2, respectively; [c] P(1) and P(2) are pattern matrixes for components 1 and 2, respectively.

From the two PCA extracts, it stands to reason that variations in sediment yield are strongly influenced by changes in agriculture, urban and forest cover. The pattern matrix (Table 8) was used to explore the relative influence of each of the individual LULC changes on sediment yield. In both components 1 and 2 of the PCA, changes in agriculture and urban lands had the strongest positive impact on sediment yield dynamics followed by forest in the first component and rangeland in the second component with a negative relationship. Findings of the study indicate that changes in agriculture and urban land covers will cause a commensurate change in sediment yield. Hooke and Sandercock [70] also assert agricultural activities and their management practices exert a strong force on erosion rates culminating in high sediment fluxes. Contrarily, the negative relationship

in the case of forest and rangeland is an indication of the inversely proportional relation between these land use types and sediment yield. Yan et al. [10] in their study found similar relationships between agriculture, urban and sediment yield as well as between forest, rangeland and sediment yield. The reduction in sediment yield in forest and rangeland areas are linked to the high evapotranspiration demands of these land cover types resulting in the reduction of overland flow (surface runoff) which is responsible for the removal of topsoil as sediments [23,35]. Similarly, the canopy structure of forested and range land areas reduces the energy of raindrops upon impact with topsoil and hence reducing the potency of raindrops in the removal of topsoil. Results of this study are in further accordance with the acknowledged role of land uses on hydrological processes which in turn affect sediment responses of river basins [20,71,72]. The differing impacts of land uses on sediment yield demonstrate that land use policies and soil erosion mitigation strategies should adopt an approach of optimized spatial distribution of land uses to minimize their impacts on basin processes.

## 4. Conclusions

The study investigated the impacts of land use and land cover changes on sediment yield in the water-stressed Olifants Basin in South Africa using hydrologic modelling and principal component analysis (PCA). Contributions of the impacts of the changes in individual land use types on sediment yield were evaluated and quantified. The results indicate that under the same climatic conditions, LULC changes accounted for about 84.7% of the variation in sediment yield. Major changes in agriculture, urban and forested areas were the key determinants in the amount of sediment produced at any given time. Changes in agriculture and urban areas corresponded positively with the changes in sediment yield; however, forested areas were identified as having an inverse relation with changes in sediment yield. The use of PCA provided useful information in assessing the impacts of LULC changes on sediment yield. Considering large-scale basins as in the case of this study, it is technically and financially unsound to monitor sediment yield at all sub-basins. It thus becomes clear that the use of emerging technologies of hydrologic models and geographic information systems (GIS) is surely the way to go. The use of these technologies provides the most practical and effective approach of spatially monitoring sediment yield in large river basins. Coupling hydrologic models and empirical statistically methods such as PCA provides the needed quantitative information critical to the decision-making process regarding land and water resources planning and management.

**Author Contributions:** The research idea was conceived by Charles Gyamfi and Julius Musyoka Ndambuki with contributions from Ramadhan Wanjala Salim. Charles Gyamfi carried out data collection, data preparation and experimentation. Preparation of the draft manuscript was done by Charles Gyamfi with Julius Musyoka Ndambuki and Ramadhan Wanjala Salim providing manuscript review and comments. All authors were involved in the final manuscript preparation and agreed to the publication of the contents of this paper.

**Conflicts of Interest:** The authors declare no conflict of interest.

## References

1. Van Rompaey, A.J.J.; Verstraeten, G.; van Oost, K.; Govers, G.; Poessen, J. Modelling mean annual sediment yield using a distributed approach. *Earth Surf. Proc. Land.* **2001**, *26*, 1221–1236. [CrossRef]

2. Akrasi, S.A. Sediment discharges from Ghanaian rivers into the sea. *West Afr. J. Appl. Ecol.* **2011**, *18*, 1–13. [CrossRef]

3. Asres, M.T.; Awulachew, S.L. SWAT based runoff and sediment yield modeling: A case study of the Gumera watershed in the Blue Nile basin. *Ecohydrol. Hydrobiol.* **2010**, *10*, 191–200. [CrossRef]

4. Basson, G.; Di Silvio, G. *Erosion and Sediment Dynamics from Catchment to Coast, a Northern Perspective and a Southern Perspective*; Technical Documents in Hydrology, No. 82; UNESCO: Paris, France, 2008.

5.　Cai, T.; Li, Q.; Yu, M.; Lu, G.; Cheng, L.; Wei, X. Investigation into the impacts of land use change on sediment yield characteristics in the upper Huaihe River basin, China. *Phys. Chem. Earth Parts A/B/C* **2012**, *53*, 1–9. [CrossRef]

6.　Wu, Y.; Chen, J. Modelling of soil erosion and sediment transport in the East River Basin in southern China. *Sci. Total Environ.* **2012**, *441*, 159–168. [CrossRef] [PubMed]

7.　Ellison, C.A.; Kiesling, R.L.; Fallon, J.D. Correlating streamflow, turbidity and suspended-sediment concentration in Minnesota's Wild River. In Proceedinds of the 2nd Joint Federal Interagency Conference, Las Vegas, NV, USA, 27 June−1 July 2010.

8.　Lu, X.X.; Ran, L.S.; Liu, S.; Jiang, T.; Zhang, S.R.; Wang, J.J. Sediment loads response to climate change: A preliminary study of eight large Chinese rivers. *Int. J. Sed. Res.* **2013**, *28*, 1–14. [CrossRef]

9.　Rovira, A.; Alcaraz, C.; Ibanez, C. Spatial and temporal dynamics of suspended load at a cross section: The lowermost Ebro River (Catalonia, Spain). *Water Res.* **2012**, *46*, 3671–3681. [CrossRef] [PubMed]

10.　Yan, B.; Fang, N.F.; Zhang, P.C.; Shi, Z.H. Impacts of land use change on watershed streamflow and sediment yield: An assessment using hydrologic modelling and partial least squares regression. *J. Hydrol.* **2013**, *484*, 26–37. [CrossRef]

11.　Boucher, K.; Van Breda Weaver, A. Sediment yield in South Africa—A preliminary geographical analaysis. *GeoJournal* **1991**, *23*, 7–17. [CrossRef]

12.　Bussi, G.; Dadson, S.J.; Prudhomme, C.; Whitehead, P.G. Modelling the future impacts of climate and land use change on suspended transport in the River Thames (UK). *J. Hydrol.* **2016**, *542*, 357–372. [CrossRef]

13.　Mullan, D. Soil erosion under the impacts of future climate change: Assessing the statistical significance of future changes and the potential on-site and offsite problems. *Catena* **2013**, *109*, 234–246. [CrossRef]

14.　Nunes, J.P.; Seixas, J.; Keizer, J.J.; Ferreira, A.J.D. Sensitivity of runoff and soil erosion to climate change in two Mediterranean watersheds. Part II: Assessing impacts from changes in storm rainfall, soil moisture and vegetation cover. *Hydrol. Process.* **2009**, *23*, 1212–1220. [CrossRef]

15.　Pruski, F.F.; Nearing, M.A. Climate-induced changes in erosion during the 21st century for eight US locations. *Water Resour. Res.* **2002**, *38*, 34-1–34-11. [CrossRef]

16.　Nearing, M.A.; Pruski, F.F.; O'Neill, M.R. Expected climate change impacts on soil erosion rates: A review. *J. Soil Water Conserv.* **2004**, *59*, 43–50.

17.　Routschek, A.; Schmidt, J.; Kreienkamp, F. Impact of climate change on soil erosion—a high-resolution projection on catchment scale until 2100 in Saxony/Germany. *Catena* **2014**, *121*, 99–109. [CrossRef]

18.　Garcia-Ruiz, J.M. The effects of land uses on soil erosion in Spain: A review. *Catena* **2010**, *81*, 1–11. [CrossRef]

19.　Boellstorff, D.; Benito, G. Impacts of set-aside policy on the risk of soil erosion in central Spain. *Agric. Ecosyst. Environ.* **2005**, *107*, 231–243. [CrossRef]

20.　Rodríguez-Lloveras, X.; Buytaert, W.; Benito, G. Land use can offset climate change induced increases in erosion in Mediterranean watersheds. *Catena* **2016**, *143*, 244–255. [CrossRef]

21.　Ward, P.J.; van Balen, R.; Verstraeten, G.; Renssen, H.; Vandenberghe, J. The impact of landuse and climate change on late Holocene and future suspended sediment yield of the Meuse catchment. *Geomorphology* **2009**, *103*, 389–400. [CrossRef]

22.　Baker, T.J.; Miller, S.N. Using the Soil and Water Assessmnent Tool (SWAT) to assess land use impact on water resources in an East African watershed. *J. Hydrol.* **2013**, *486*, 100–111. [CrossRef]

23.　Fohrer, N.; Haverkamp, S.; Eckhardt, K.; Frede, H.G. Hydrologic response to land use changes on the catchment scale. *Phys. Chem. Earth Part B Hydrol. Oceans Atmos.* **2001**, *26*, 577–582. [CrossRef]

24.　Nie, W.; Yuan, Y.; Kepner, W.; Nash, M.S.; Jackson, M.; Erickson, C. Assessing impacts of land use and land cover changes on hydrology for the upper San Pedro watershed. *J. Hydrol.* **2011**, *407*, 105–114. [CrossRef]

25.　Wang, S.; Kang, S.; Zhang, L.; Li, F. Modelling hydrological response to different land use and climate change scenarios in the Zamu River basin of the northwest China. *Hydrol. Process.* **2008**, *22*, 2502–2510. [CrossRef]

26.　Lazzari, M.; Gioia, D.; Piccarreta, M.; Danese, M.; Lanorte, A. Sediment yield and erosion rate estimation in the mountain catchments of the Camastra artificial reservoir (Southern Italy): A comparison between different empirical methods. *Catena* **2015**, *127*, 323–339. [CrossRef]

27.　Van Rompaey, A.; Bazzoffi, P.; Jones, R.J.A.; Montanarella, L. Modeling sediment yields in Italian catchments. *Geomorphology* **2005**, *65*, 157–169. [CrossRef]

28.　Thomas, R.B. Estimating total suspended sediment yield with probability sampling. *Water Resour. Res.* **1985**, *21*, 1381–1388. [CrossRef]

29. Oeurng, C.; Sauvage, S.; Sanchez-Perez, J. Assessment of hydrology, sediment and particulate organic carbon yield in a large agricultural catchment using the SWAT model. *J. Hydrol.* **2011**, *401*, 145–153. [CrossRef]

30. Tattari, S.; Rekolainen, B.S.; Posch, M.; Siimes, K.; Tuhkanen, H.-R.; Yli-Halla, M. Modelling sediment yield and phosphorus transport in Finnish Clayey soils. *Trans. ASAE* **2001**, *44*, 297–307. [CrossRef]

31. Bussi, G.; Frances, F.; Horel, E.; Lopez-Tarazon, J.A.; Batalla, R.J. Modelling the impact of climate change on sediment yield in a highly erodible Mediterranean catchment. *J. Soils Sediments* **2014**, *14*, 1921–1937. [CrossRef]

32. Bussi, G.; Rodriguez-Lloveras, X.; Frances, F.; Benito, G.; Sanchez-Moya, Y.; Sopena, A. Sediment yield model implementation based on check dam infill stratigraphy in a semiarid Mediterranean catchment. *Hydrol. Erath Syst. Sci.* **2013**, *17*, 3339–3354. [CrossRef]

33. Yesuf, H.M.; Assen, M.; Alamirew, T.; Melesse, A.M. Modeling of sediment yield in Maybar gauged watershed using SWAT, northeast Ethiopia. *Catena* **2015**, *127*, 191–205. [CrossRef]

34. Setegn, S.G.; Dargahi, B.; Srinivasan, R.; Melesse, A.M. Modelling of sediment yield from Anjeni-Gauged watershed, Ethiopia using SWAT model. *J. Am. Water Resour. Assoc.* **2010**, *46*, 514–526. [CrossRef]

35. Shi, Z.H.; Ai, L.; Li, X.; Huang, X.D.; Wu, G.L.; Liao, W. Partial least squares regression for linking landcover patterns to soil erosion and sediment yield in watersheds. *J. Hydrol.* **2013**, *498*, 165–176. [CrossRef]

36. Rooseboom, A. *Sediment Transport in Rivers and Reservoirs. A Southern African Perspective*; WRC Report No. 297/1/92; Water Research Commission: Pretoria, South Africa, 1992.

37. International Water Management Institute. *Baseline Report Olifants River Basin in South Africa: A contribution to the Challenge Program Project 17. Integrated Water Resource Management for Improved Rural Livelihoods: Managing Risk, Mitigating Drought and Improving Water Productivity in the Water Scarce Limpopo Basin*; IWMI: Pretoria, South Africa, 2008.

38. Schulze, R.E.; Maharaj, M.; Lynch, S.D.; Howe, B.J.; Melvil-Thomson, B. *South African Atlas for Agrohydrology and Climatology*; University of KwaZulu-Natal: Pietermaritzburg, South Africa, 1997.

39. Gyamfi, C.; Ndambuki, J.M.; Salim, R.W. A historical analaysis of rainfall trend in the Olifants Basin in South Africa. *Earth Sci. Res.* **2016**, *5*, 129–142. [CrossRef]

40. Food and Agriculture Organization. *Digital Soil Map of The World and Derived Soil Properties*; FAO: Rome, Italy, 2005.

41. Department of Water Affairs And Forestry. *Olifants Water Management Area: Internal Strategic Perspective*; Report No. P WMA 04/000/00/0304; Department of Water Affairs and Forestry: Pretoria, South Africa, 2004.

42. Department of Water Affairs And Forestry. *Olifant River Water Resources Development (ORWRP) Environmental Impact Assessment (12/12/20/553)*; Infrastucture Development, DWAF: Pretoria, South Africa, 2005.

43. Ghaffari, G.; Keesstra, S.; Ghodousi, J.; Ahmadi, H. SWAT—simulated hydrological impact of land use change in the Zanjanrood Basin, Northwest Iran. *Hydrol. Process.* **2010**, *24*, 892–903. [CrossRef]

44. Arnold, J.G.; Fohrer, N. Current capabilities and research opportunities in applied watershed modeling. *Hydrol. Process.* **2005**, *19*, 563–572. [CrossRef]

45. Arnold, J.G.; Srinivasan, R.; Muttiah, R.S.; Williams, J.R. Large area hydrologic modeling and assessment—Part 1: Model development. *J. Am. Water Resour. Assoc.* **1998**, *34*, 73–89. [CrossRef]

46. Williams, J.R. The EPIC model. In *Computer Models of Watershed Hydrology*; Singh, V.P., Ed.; Water Resouces Publication: Highlands Ranck, CO, USA, 1995; pp. 909–1000.

47. Neitsch, S.L.; Arnold, J.G.; Kiniry, J.R.; Williams, J.R. *SWAT User Manual (Version 2009)*; Texas Water Resources Institute Technical Report; Texas A and M University: Temple, TE, USA, 2011.

48. Bagnold, R.A. Bedload transport in natural rivers. *Water Resour. Res.* **1977**, *13*, 303–312. [CrossRef]

49. Williams, J.R. SPNM, a model for predicting sediment, phosphors and nitrogen yields from agricultural watersheds. *Water Resour. Bull.* **1980**, *16*, 843–848. [CrossRef]

50. Food and Agriculture Organization. *Major Soils of The World. Land and Water Digital Media Series*; FAO: Rome, Italy, 2002.

51. Land Type Survey Staff. *Land Types of South Africa: Digital Map (1:250 000 Scale) and Soil Inventory Datasets (1972–2006)*; ARC-Institute for Soil, Climate and Water: Pretoria, South Africa, 1972–2006.

52. Batjes, N.H. *ISRIC-WISE Global Data Set of Derived Soil Properties on a 0.5 by 0.5 Degree Grid (Version 2.0)*; Report 2002/03; International Soil Reference and Information Centre (ISRIC): Wageningen, The Netherlands, 2002.

53. Anderson, J.R.; Hardy, E.E.; Roach, J.T.; Witmer, W.E. *A Land Use and Land Cover Classification System for Use with Remote Sensor Data*; USGS (United States Geological Survey): Washington, VI, USA, 1976; Volume 964, pp. 138–145.

54. Food and Agriculture Organization. *The Digital Soil Map of The World (Version 3.6)*; FAO: Rome, Italy, 2003.

55. Abbaspour, K.C. *SWAT-CUP-2012. SWAT Calibration and Uncertainty Program—A User Manual*; Swiss Federal Institute of Aquatic Science and Technology: Dubendorf, Switzerland, 2012.

56. Moriasi, D.N.; Arnold, J.G.; van Liew, M.W.; Bingner, R.L.; Harmel, R.D.; Veith, T.L. Model evaluation guidelines for systematic quantification of accuracy in Watershed Simulations. *Trans. ASABE* **2007**, *50*, 885–900. [CrossRef]

57. Santhi, C.; Arnold, J.G.; Williams, J.R.; Dugas, W.A.; Hauck, L. Validation of the SWAT model on a large river basin with point and nonpoint sources. *J. Am. Water Resour. Assoc.* **2001**, *37*, 1169–1188. [CrossRef]

58. Nash, J.E.; Sutcliffe, J.V. River flow forecasting through conceptual models. Part I-a discussion of principles. *J. Hydrol.* **1970**, *10*, 282–290.

59. Gupta, H.V.; Sorooshian, S.; Yapo, P.O. Status of automatic calibration for hydrologic models: Comparison with multilevel expert calibration. *J. Hydrol. Eng.* **1999**, *4*, 135–143. [CrossRef]

60. Lin, B.; Chen, X.; Yao, H.; Chen, Y.; Liu, M.; Gao, L.; James, A. Analysis of landuse change impacts on catchment runoff using different time indicators based on SWAT model. *Ecol. Indic.* **2015**, *58*, 55–63. [CrossRef]

61. Tang, L.H.; Yang, D.W.; Hu, H.P.; Gao, B. Detecting the effect of land use change on streamflow, sediment and nutrient losses by distributed hydrological simulation. *J. Hydrol.* **2011**, *409*, 172–182. [CrossRef]

62. Wang, G.; Xia, J.; Chen, J. Quantification of the effects of climate variations and human activities on runoff by a monthly water balance model: A case study of the Chaobai River Basin in Northern China. *Water Resour. Res.* **2009**, *45*, 1–12. [CrossRef]

63. Lahmer, W.; Pfiitzner, B.; Becker, A. Assessment of landuse and climate change impacts on the mesoscale. *Phys. Chem. Earth* **2001**, *26*, 565–575. [CrossRef]

64. Hu, Q.; Willson, G.D.; Chen, X.; Akyuz, A. Effects of climate and landcover change on stream discharge in the Ozark highlands USA. *Environ. Model. Assess.* **2004**, *10*, 9–19. [CrossRef]

65. Rooseboom, A. Sediment transport in Southern African rivers. *Water SA* **1978**, *4*, 14–17.

66. Rooseboom, A.; Verster, E.; Zietsman, H.L.; Lotriet, H.H. *The Development of The New Sediment Yield Map of South Africa*; WRC Report NO. 297/2/92; Water Research Commission: Pretoria, South Africa, 1992.

67. Milliman, J.D.; Farnsworth, K.L. *River Discharge to The Coastal Ocean: A Global Synthesis*; Cambridge University Press: Cambridge, UK, 2011; p. 384.

68. Bolton, P. Sediment Deposition in Major Reservoirs in the Zambezi Basin. Available online: http://hydrologie.org/redbooks/a144/iahs_144_0559.pdf (accessed on 14 October 2016).

69. Food and Agriculture Organization. Global River Sediment Yields Database. Available online: http://www.fao.org/nr/water/aquastat/sediment/index.stm (accessed on 11 October 2016).

70. Hooke, J.; Sandercock, P. Use of vegetation to combat desertification and land degradation: Recommendations and guidelines for spatial strategies in Mediterranean lands. *Landsc. Urban Plan.* **2012**, *107*, 389–400. [CrossRef]

71. Benyon, R.G.; Theiveyanathan, S.; Doody, T.M. Impacts of tree plantations on groundwater in south-eastern Australia. *Aust. J. Bot.* **2006**, *54*, 181–192. [CrossRef]

72. Chase, T.N.; Pielke, R.A., Sr.; Kittel, T.G.F.; Nemani, R.R.; Running, S.W. Simulated impacts of historical land cover changes on global climate in northern winter. *Clim. Dyn.* **2000**, *16*, 93–105. [CrossRef]